Rollins Chris (Orcid ID: 0000-0002-5291-6956)

Avouac Jean-Philippe (Orcid ID: 0000-0002-3060-8442)

A geodesy- and seismicity-based local earthquake likelihood model for central Los Angeles

Chris Rollins[1*] and Jean-Philippe Avouac[1]

Abstract

We estimate time-independent earthquake likelihoods in central Los Angeles using a model of interseismic strain accumulation and the 1932-2017 seismic catalog. We assume that on the long-term average, earthquakes and aseismic deformation collectively release seismic moment at a rate balancing interseismic loading, mainshocks obey the Gutenberg-Richter law (a log-linear magnitude-frequency distribution (MFD)) up to a maximum magnitude and a Poisson process, and aftershock sequences obey the Gutenberg-Richter and "Bâth" laws. We model a comprehensive suite of these long-term systems, assess how likely each system would be to have produced the MFD of the instrumental catalog, and use these likelihoods to probabilistically estimate the long-term MFD. We estimate M_{max}=6.8 +1.05/-0.4 (every ~300 years) or M_{max}=7.05 +0.95/-0.4 assuming a truncated or tapered Gutenberg-Richter MFD, respectively. Our results imply that, for example, the (median) likelihood of a Mw≥6.5 mainshock is 0.2% in one year, 2% in 10 years, and 18-21% in 100 years.

[1]Division of Geological and Planetary Sciences, California Institute of Technology, Pasadena, CA, USA.

*Now at Department of Earth and Environmental Sciences, Michigan State University, East Lansing, MI, USA; rollin32@msu.edu.

Key Points

- We develop a method to probabilistically estimate long-term earthquake likelihoods using a strain buildup model and a seismic catalog
- We infer that the maximum-magnitude earthquake in central Los Angeles is Mw=6.8 +1.05/-0.4 or Mw=7.05 +0.95/-0.4 depending on assumptions
- Our results can be used, for example, to estimate the probability of having an earthquake of or exceeding any magnitude in any timespan

This article has been accepted for publication and undergone full peer review but has not been through the copyediting, typesetting, pagination and proofreading process which may lead to differences between this version and the Version of Record. Please cite this article as doi: 10.1029/2018GL080868

1. Introduction

The transpressional 'Big Bend' of the San Andreas Fault (Figure 1c) induces north-south tectonic shortening across Los Angeles (LA) that is released in thrust earthquakes such as the damaging 1971 Mw~6.7 Sylmar, 1987 Mw~5.9 Whittier Narrows and 1994 Mw=6.7 Northridge shocks [e.g. Dolan et al., 1995]. Paleoseismologic studies have also found evidence of possible Holocene Mw≥7.0 earthquakes on several thrust faults in greater LA [Rubin et al., 1998; Leon et al., 2007, 2009] (Figure 1a). In principle, one can quantify the likelihoods of future earthquakes on these faults by using geodetic data to assess how quickly elastic strain is accumulating on them and employing the elastic rebound hypothesis [Reid, 1910], which implies that they should release strain at this same rate on the long-term average. The strain accumulation can also be expressed as a deficit of seismic moment, which can be assumed to be balanced over the long term by the moment released in earthquakes and aseismic slip [Brune, 1968; Molnar, 1979; Avouac, 2015]. This approach has found use in several regional and global studies [e.g. Shen et al., 2007; Rong et al., 2014; Hsu et al., 2016; Stevens and Avouac, 2016, 2017; Michel et al., 2018].

Applying this approach to LA is challenging, in part because the task of assessing strain buildup rates encounters several unique hurdles there: some of the thrust faults are blind (do not break the surface), obscuring strain accumulation on them [Lin and Stein, 1989; Stein and Yeats, 1989; Shaw and Suppe, 1996]; the geodetic data are affected by deformation related to aquifer and oil use [Argus et al., 2005; Riel et al., 2018]; and central LA sits atop a deep sedimentary basin that introduces a first-order elastic heterogeneity [Shaw et al., 2015]. In recent work, Rollins et al [2018] addressed these three challenges and modeled the north-south shortening as resulting from interseismic strain buildup on the upper sections of the north-dipping Sierra Madre, Puente Hills and Compton thrust faults (Figure 1a), implying that a deficit of seismic moment accrues at a total rate of 1.6 +1.3/-0.5 x 10^{17} Nm/yr (Figure 1b). This model assumes that deformation updip of the blind Compton and Puente Hills faults is anelastic and aseismic; the total moment deficit buildup rate would be 2.4 +1.3/-0.6 x 10^{17} Nm/yr if this deformation were instead elastic (Figure 1b), but this seems unlikely in view of the depth distribution of seismicity [Rollins et al., 2018]. The 1.6 x 10^{17} Nm/yr moment deficit could be all released by a Mw=7.0 earthquake every 240 years, for example, but this cannot form a basis for seismic hazard assessment as 1) the choice of magnitude is arbitrary and 2) it overlooks the contributions of smaller (and possibly larger) events and aseismic slip. Here we develop a probabilistic estimate of long-term-average earthquake likelihoods by magnitude in central LA that accounts for these factors, using the moment deficit buildup rate and the seismic catalog.

2. Moment buildup vs. release in earthquakes

We first assess whether this moment deficit has been balanced by the collective moment release in small, moderate and large earthquakes over the period of the instrumental catalog [e.g. Meade and Hager, 2005; Stevens and Avouac, 2016]. We use locations and magnitudes from the 1932-2017 Southern California Earthquake Data Center (SCEDC) catalog within a study area defined by the geometries of the Sierra Madre, Puente Hills and Compton faults and an inferred master decollement [Fuis et al., 2001; Shaw et al, 2015; Rollins et al., 2018] (Figure 1a, thin dashed lines). The 1933 M_w~6.4 Long Beach and 1971 M_w~6.7 Sylmar earthquakes occurred on the edges of the study area (Figure 1a); we handle this ambiguity by using four versions of the instrumental catalog that alternatively include or exclude them and their aftershocks (Supporting Information S1). (We exclude the 1994 Northridge earthquake, which occurred further west.) We compare moment buildup and release in 1932-2017 over a

range of upper cutoff magnitudes for the earthquakes so as to qualitatively assess how large earthquakes need to get in central LA to collectively balance the "moment budget." The answer visibly depends on whether the 1933 and 1971 earthquakes are counted or not (Figure 2). This technical issue hints at the reason why this comparison has limited predictive power: the instrumental catalog (e.g. exactly one Mw~6.4 and one Mw~6.7 earthquake) does not simply repeat every 86 years, but rather is an 86-year realization of an ongoing process. (This method also ignores the moment released by undetected small earthquakes, which may be nonnegligible.)

3. The Gutenberg-Richter relation, long-term models, and a new approach

A way around these issues is to assume that on the long-term average, 1) the geodetic moment deficit buildup rate is constant and is balanced by earthquakes and aseismic deformation, and 2) earthquakes obey the Gutenberg-Richter (G-R) law, meaning that their magnitude-frequency distribution (MFD) is log-linear with slope *-b* [Gutenberg and Richter, 1954]. If the G-R distribution is additionally assumed to hold up to a maximum earthquake magnitude M_{max}, the long-term MFD is uniquely determined by the moment buildup rate, *b*, M_{max} and the aseismic contribution [Molnar, 1979; Avouac, 2015]. We work with two alternate closed-form MFD solutions: a truncated G-R distribution (Supporting Information S2) and a "tapered" G-R distribution (Supporting Information S3). In the 2D space of M_w vs. log-frequency of earthquakes of or exceeding that M_w, which we call Gutenberg-Richter space, the truncated G-R distribution is a line that ends at M_{max} (Figure S1a, S2a), while the tapered G-R distribution tapers to $-\infty$ at M_{max} (Figure S1c, S2f). These may be suitable endmembers: the truncated G-R distribution in fact implies a mix of log-linear and characteristic behavior (Figure S1a, Supporting Information S2); the tapered G-R distribution (which implies no characteristic element) follows from a different use of the log-linear relation (Supporting Information S3) and does not require specifying a form for the tapering [e.g., Jackson and Kagan, 1999]; and both are log-linear in Gutenberg-Richter space except at or near M_{max} and therefore may be reconcilable with observations in most settings.

However, several challenges remain in this approach. First, M_{max} is unknown due to the short history of observation. Some studies iteratively estimate M_{max} in cumulative magnitude-frequency space [Stevens and Avouac, 2016, 2017]; others estimate it using total fault areas and scaling relations [Field et al., 2014] or assume a value for the maximum earthquake's recurrence interval [Hsu et al., 2016]. Second, while some studies estimate *b a priori* from the catalog [Field et al., 2014; Stevens and Avouac, 2016, 2017], it is desirable to fully account for the covariances between *b*, M_{max}, the moment deficit buildup rate and other factors in estimating long-term earthquake rates. Third, it is uncertain whether to decluster the instrumental catalog first [Michel et al., 2018], which method to use if so, whether declustering should yield a smaller b-value [Felzer, 2007; Marsan and Lengline, 2008], and how this may affect the inferred long-term model.

Here we develop a probabilistic method to estimate long-term earthquake rates that handles these challenges (Figures S1-S2, Supporting Information S2-S5). We generate a large suite of moment-balancing long-term models (described by MFDs), use each to populate a set of synthetic 86-year earthquake catalogs, and compare the synthetic MFDs to that of the 86-year-long SCEDC catalog to evaluate how likely the 1932-2017 seismicity would be to arise as an 86-year realization of each long-term process. We generate the long-term models by iterating over a wide range of values of *b* and M_{max} and over the probability density function (PDF) of moment deficit accumulation rate (Figure 1b) and computing the moment-balancing truncated or tapered G-R MFD under each combination of parameters (Supporting Information

S2-3). Following Michel et al. [2018], we incorporate "Bâth's law," the observation that the largest aftershock is often ~1.2 magnitude units smaller than the mainshock [Bâth, 1965]. To do so, we assume that it is mainshocks (not all earthquakes) that obey the truncated or tapered G-R form described by *b*, and that each mainshock is then individually accompanied by aftershocks obeying their own truncated G-R distribution (described by the same *b*) up to a single aftershock 1.2 magnitude units below the mainshock. The moment contribution of aftershocks is then a constant (Supporting Information S4), and the parameter *b* is essentially the "declustered" (mainshocks-only) b-value, which we have also assumed governs individual aftershock sequences. We assume that each mainshock is also followed by aseismic deformation that releases 25% as much moment as the mainshock, based on inferences from the Northridge earthquake [Donnellan et al., 1998]. We then use each long-term MFD to populate a set of 25 synthetic 86-year catalogs assuming that mainshocks of each magnitude obey a Poisson process and adding their aftershocks. We compute the misfit of the 25 synthetic catalogs' cumulative MFDs to those of the four versions of the 1932-2017 catalog in Gutenberg-Richter space (Figure S2b-d), convert these misfits to Gaussian likelihoods, and use these likelihoods to compute the PDFs of key parameters and long-term earthquake rates (Supporting Information S5). In a truncated G-R distribution, these parameters also define $T(M_{max})$, the maximum earthquake's recurrence interval, so we estimate the 2D PDF of M_{max} and $T(M_{max})$; in a tapered G-R distribution, $T(M_{max})$ is infinite and so we only estimate the 1D PDF of M_{max}. This method has the advantages that 1) it directly tests long-term models based on whether the instrumental catalog is a plausible realization of each long-term process, 2) *b* and M_{max} are estimated *a posteriori* with full covariance with other variables, and 3) it does not require declustering the catalog.

4. Results

We first describe our two preferred long-term average earthquake likelihood models (Figure 3), which respectively assume a truncated and a tapered G-R distribution for mainshocks. In the truncated case, the 2D PDF of M_{max} and $T(M_{max})$ peaks at a M_w=6.75 event with a recurrence interval of ~280 yr. The weighted 16th- and 84th-percentile recurrence intervals of the maximum earthquake for M_{max}=6.75 are 170 and 610 yr; the 1D PDF of M_{max} (mode and same percentiles) is M_w=6.8 +1.05/-0.4 (Figure 3a). In the tapered case, the 1D PDF of M_{max} gives M_w=7.05 +0.95/-0.4. (M_{max} is always ~0.25 larger in the tapered models because the tapering requires a larger M_{max} to close the moment budget.) The aggregate mean magnitude and recurrence interval of paleoseismologically inferred Holocene earthquakes on the Sierra Madre, Puente Hills and Compton faults are respectively M_w=7.31 ± 0.24 and 920 +100/-80 years (Figure 3a, brown errorbars). While our PDFs for M_{max} peak at smaller magnitudes, they do not exclude the possibility of such large earthquakes: the likelihood of M_{max} being ≥M_w=7.3 is respectively 38% and 47% in the truncated and tapered estimates. (The paleomagnitudes were also estimated using scaling relations based on both strike-slip and thrust earthquakes and would be ~0.5 lower if relations based only on thrust earthquakes were used [Leon et al., 2009].) In both estimates, the full MFDs (including aftershocks) of the lowest-misfit long-term-average models (Figure 3a, thin translucent gray and blue lines) are comparable to the instrumental MFDs at smaller magnitudes (brown lines). The lowest-misfit full MFDs are also comparable to the sum of the cumulative nucleation MFDs on all faults in the study area from the Uniform California Earthquake Rupture Forecast, Version 3 (UCERF3) [Field et al., 2014] (Figure 3a, dashed purple line) except that the UCERF3 MFD goes to higher magnitudes (see Discussion). The intrinsic model parameter *b* (governing mainshocks) in the lowest-misfit models peaks at 0.8-0.9 (Figure 3b, solid blue and gray lines), close to the statewide

declustered value of b=0.85 ±0.13 [Felzer, 2007]. The maximum-likelihood (M_c=3.5) effective b-values of the full long-term MFDs (including aftershocks) in the lowest-misfit models peak at 0.9-1.0 (Figure 3b, dashed blue and gray), consistent with the maximum-likelihood b-values of the four versions of the instrumental catalog (Figure 3b, brown lines) and with the Hutton et al. [2010] estimate of b=1.0 for Southern California. The effective b-values may peak slightly below 1.0 because the aftershock sequences of the 1987 Whittier Narrows and 1991 Mw~5.8 Sierra Madre earthquakes had respective b-values of 0.67 and 0.6 [Hauksson and Jones, 1989; Hauksson, 1994] and are in all four versions of the instrumental catalog constraining these models.

These preferred models apply equal weighting to the four versions. We assess the effect of this by generating four alternate estimates each calibrated to only one version. We find that the version used has a substantial but intuitive effect on M_{max}. The version that excludes the 1933 and 1971 events and their aftershocks features relatively low earthquake rates (and fell far short of balancing the 86-year moment budget on its own (Figure 2, white line)), and so the model must add more large, infrequent earthquakes to balance the long-term-average moment budget: M_{max}=7.15 +1.0/-0.45 and M_{max}=7.3 +0.9/-0.35 for the truncated and tapered cases, respectively (Figure S3d). The subcatalog that counts both the 1933 and 1971 sequences, by contrast, features much higher small and moderate earthquake rates and so large earthquakes are not needed in the long-term moment budget: M_{max}=6.4 +1.05/-0.2 (truncated) and M_{max}=6.65 +0.95/-0.3 (tapered) (Figure S3a). The estimates using versions that count one sequence or the other lie in the middle of these two, as might be expected (Figure S3b,c).

If we assume that postseismic deformation is nonexistent and 100% of moment release occurs in earthquakes, larger earthquakes are needed to close the moment budget: M_{max}=6.95 +1.05/-0.45 (truncated) and M_{max}=7.2 +0.85/-0.45 (tapered) (Figure S4a). If we alternatively assume that strain accumulation updip of the Puente Hills and Compton faults is elastic, the moment deficit buildup is ~50% faster (Figure 1b, red line) and so M_{max}=7.1 +0.95/-0.4 (truncated) and M_{max} = 7.35 +0.8/-0.45 (tapered) (Figure S4b). We can also relax the mainshock-aftershock distinction and assume instead that all earthquakes obey a single G-R distribution characterized by the intrinsic parameter *b* (which is then the b-value of the full MFD) and Poisson recurrence. This yields a similar long-term model, with M_{max}=6.9 +1.05/-0.45 (truncated) and M_{max} = 7.15 +0.9/-0.5 (tapered) (Figure S5a), and *b*=0.9-1.0 in the lowest-misfit models (Figure S5b), consistent with the maximum-likelihood full b-value in the preferred models (Figure 3b).

5. Implications for earthquake likelihoods in Los Angeles

Our preferred models (Figure 3) can be used, for example, to estimate the likelihood of observing at least one mainshock of at least a given magnitude in a given time period (Supporting Information S6). Assuming that mainshocks of each magnitude follow a Poisson process, the weighted-median probability of observing at least one Mw≥6.0 mainshock is 59% in 100 years, 8.5% in 10 years, and 0.9% in 1 year for the truncated G-R model, or 62% in 100 years, 9.3% in 10 years, and 1.0% in 1 year for the tapered model (Figure 4). The likelihoods are similar if one assumes that mainshocks follow a Brownian renewal process [Matthews et al., 2002; Field and Jordan, 2015] (Figure S6). The weighted-median probability of at least one Mw≥6.5 mainshock assuming a Poisson process is 18% in 100 years, 2.0% in 10 years, and 0.2% in 1 year (truncated) or 21%, 2.3% and 0.2% (tapered). The probability of observing three or more Mw≥5.9 mainshocks in 86 years is 7.5% (truncated) or 9.4% (tapered), suggesting that it is rather unlikely to have observed three earthquakes like the Mw~6.7

Sylmar, Mw~6.4 Long Beach and Mw~5.9 Whittier Narrows shocks in the 86-year instrumental period. Even counting aftershocks, the rates of earthquakes of or exceeding those magnitudes are still several times lower in these models than in the catalog (Figure 3a). In order words, according to these models, central LA has experienced a relative abundance of Mw≥5.9 earthquakes in the instrumental era. We note that the instrumental era may have followed a relatively quiet period (although incompleteness issues make this somewhat speculative): Toppozada [2002] reports only two Mw≥6 earthquakes in central LA between 1769 and 1932, and one of them, the 1769 earthquake felt by the Portola expedition, may have in fact occurred in Orange County [Grant et al, 2002], leaving only a M~6 earthquake in 1855 in the study area [Yerkes, 1985]. If one downward-adjusts the instrumental MFD above Mw=5.9 by adding only one Mw=6.0 earthquake in 163 years, the total MFD (Figure 3a, dashed brown line) more closely matches our long-term model and the UCERF3 nucleation MFD. If one adds this quiescence to the entire instrumental MFD and then reruns our method, M_{max} rises to M_w=7.15 +0.85/-0.4 (truncated) or M_w=7.45 +0.65/-0.45 (tapered) (Figure S4c).

6. Discussion/Conclusion

Our method for probabilistically estimating long-term earthquake likelihoods satisfies the moment conservation principle, accounts for a broad range of data and considerations, and can be used in probabilistic seismic hazard assessment anywhere. It has features in common with relatively successful existing forecasts, such as the separation of mainshocks and aftershocks [Helmstetter et al., 2007], use of geodetic data [Field et al., 2014; Bird et al., 2015], and model tuning based on retrospective prediction of seismic catalogs [Bird et al., 2015]. However, our approach has the advantage of estimating *b*, M_{max} and long-term earthquake likelihoods *a posteriori* with full covariance. Our results may not be unreasonable: an earthquake rupturing the entire Sierra Madre Fault, for example, would have magnitude M=7.26 or M=7.40 using empirical scaling relations from Wells and Coppersmith [1994] (thrust events only) or Hanks and Bakun [2008], respectively. This is similar to our M_{max}=7.2 +0.85/-0.45 tapered G-R estimate assuming 100% of slip occurs seismically (Figure S4a) even though these scaling relations are independent of strain buildup (and the Sierra Madre is not likely locked over its full area [Rollins et al., 2018].)

Several caveats are nevertheless worth noting. First, our approach is not only time-independent (it does not incorporate the time distribution of earthquakes in the SCEDC catalog, for example) but also operates on long-term averages. Even if the estimated PDF of M_{max} and $T(M_{max})$ were a 2D delta function at Mw=6.75 and 280 years, for example, this would not imply that larger earthquakes should never occur, only that they would likely overshoot the moment budget (given the rest of the model) and should on average be balanced by relative quiescence. The timescale over which this balance may exist is unknown, as large earthquakes may cluster in time over thousands of years [McCalpin et al., 1996, Rockwell et al., 2000, Dolan et al., 2007, Benedetti et al., 2013], and so the large inferred paleoearthquakes could also be features of a system of which our models are a long-term average. Second, we assume that interseismic deformation rates are time-independent, which may be untrue [e.g., Mavrommatis et al., 2014; Tsang et al., 2015]. Third, we assume that all earthquakes are either inside or outside the study area, which belies the possibility of a large multifault earthquake nucleating in LA and propagating outside. Fourth, we also assume that the earthquakes only release strain from north-south shortening; although this is the principal strain in LA [Zoback et al., 1987], it is only a component of the relative plate motion. These two factors may explain why the cumulative local UCERF3 nucleation MFD has a larger M_{max} than our preferred model (Figure 3b). (In UCERF2, which did not incorporate multifault ruptures, the

inferred M_{max} on the Sierra Madre and Puente Hills faults was ~0.5 lower [Field et al., 2007]). Fifth, while the truncated G-R distribution does imply an element of characteristic behavior at M_{max} (Figure S1a, Supporting Information S2), which we find lowers the estimated M_{max} by ~0.25 compared to the tapered distribution, we do not explore more characteristic MFDs like those inferred by UCERF3. Finally, our method would require adjustment (and denser geodetic data or other constraints) in order to be separable into single-fault forecasts.

Acknowledgements

C. Rollins was supported by a NASA Earth and Space Science Fellowship for most of this work. The authors are grateful to Tom Parsons and an anonymous reviewer for suggestions that greatly improved the manuscript, as well as numerous colleagues around the community for helpful input and guidance. The authors declare no competing financial interests. The GPS data used to constrain the moment deficit buildup rate in Rollins et al. [2018] and plotted in Figure 1 can be found in Argus et al. [2005], table 3; the SCEDC seismic catalog is available at http://service.scedc.caltech.edu/ftp/catalogs/SCEC_DC/.

References

Aki, K. (1965). Maximum Likelihood Estimate of b in the Formula log N = a – bM and its Confidence Limits. *Bull. Earth. Res. Inst.* **43**, 237-239.

Argus, D. F., Heflin, M. B., Peltzer, G., Crampé, F. & Webb, F. H. (2005). Interseismic strain accumulation and anthropogenic motion in metropolitan Los Angeles. *J. Geophys. Res.* **110**(B4).

Avouac, J.-P. (2015). From geodetic imaging of seismic and aseismic fault slip to dynamic modeling of the seismic cycle. *Ann. Rev. Earth Plan. Sci.* **43**, 233-271.

Båth, M. (1965). Lateral inhomogeneities of the upper mantle. *Tectonophys.* **2**(6), 483-514.

Benedetti, L., Manighetti, I., Gaudemer, Y., Finkel, R., Malavieille, J., Pou, K., Arnold, M., Aumaître, G., Bourlès, D., & Keddadouche. K. (2013). Earthquake synchrony and clustering on Fucino faults (Central Italy) as revealed from in situ 36Cl exposure dating. J*. Geophys. Res.* **118**(9), 4948-4974.

Brune, J. N. (1968). Seismic moment, seismicity, and rate of slip along major fault zones. *J. Geophys. Res.* **73**(2), 777-784.

Dolan, J. F., Sieh, K., Rockwell, T. K., Yeats, R. S., Shaw, J., Suppe, J., Huftile, G. J., & Gath, E. M. (1995). Prospects for larger or more frequent earthquakes in the Los Angeles metropolitan region. *Science* **267**, 199-205.

Dolan, J. F., Bowman, D. D. & Sammis, C.G. (2007). Long-range and long-term fault interactions in Southern California. *Geology* **35**(9), 855:858.

Donnellan, A. & Lyzenga, G. A. (1998). GPS measurements of fault afterslip and upper crustal deformation following the Northridge earthquake. *J. Geophys. Res.* **103**(B9), 21285-21297.

England, P. & Bilham, R. (2015). The Shillong Plateau and the great 1897 Assam earthquake. *Tectonics* **34**, 1792-1812.

Felzer, K. R. (2007). Appendix I: Calculating California Seismicity Rates. In "The Uniform California Earthquake Rupture Forecast, Version 2 (UCERF2)." USGS Open-File Report 2007-1437I.

Field, E. H., Dawson, T. E., Felzer, K. R., Frankel, A., Gupta, P., Jordan, T. H., Parsons, T., Petersen, M. T., Stein, R. S., Weldon, R. J., & Wills, C. J. (2007). The Uniform California Earthquake Rupture Forecast, Version 2 (UCERF2). USGS Open-File Report 2007-1437I.

Field, E. H., Arrowsmith, R. J., Biasi, G. P., Bird, P., Dawson, T. E., Felzer, K. R., Jackson, D. D., Johnson, K. M., Jordan, T. H., Madden, C., Michael, A. J., Milner, K. R., Page, M. T., Parsons, T., Powers, P. M., Shaw, B. E., Thatcher, W. R., Weldon, R. J., & Zeng, Y. (2014). Uniform California earthquake rupture forecast, version 3 (UCERF3)—The time- independent model. *Bull. Seis. Soc. Am.* **104**(3), 1122-1180.

Field, E. H. & Jordan, T. H. (2015). Time-dependent renewal-model probabilities when date of last earthquake is unknown. *Bull. Seis. Soc. Am.* **105**(1), 459–463.

Fuis, G., Ryberg, T., Godfrey, N., Okaya, D. & Murphy, J. (2001). Crustal structure and tectonics from the Los Angeles basin to the Mojave Desert, southern California. *Geology* **29(**1), 15-18.

Grant, L. B., Ballenger, L. J. & Runnerstrom, E. E. (2002). Coastal uplift of the San Joaquin Hills, southern Los Angeles Basin, California, by a large earthquake since AD 1635. *Bull. Seis. Soc. Am.* **92**(2), 590-599.

Gutenberg, B. & Richter, C. F. (1954). *Seismicity of the Earth and Associated Phenomena* (Princeton University Press, Princeton, N.J.).

Hanks, T. H., & Bakun, W. H. (2008). M-log A Observations for Recent Large Earthquakes. *Bull. Seis. Soc. Am.* **98**(1), 490-494.

Hauksson, E. & Jones, L. M. (1989). The 1987 Whittier Narrows Earthquake Sequence in Los Angeles, Southern California, Seismological and Tectonic Analysis. *J. Geophys. Res.* **94**(B7), 9569-9589.

Hauksson, E. (1994). The 1991 Sierra Madre earthquake sequence in southern California: Seismological and tectonic analysis. *Bull. Seis. Soc. Am.* **84**(4), 1058-1074.

Hauksson, E., Yang, W., & Shearer, P. M. (2012). Waveform relocated earthquake catalog for southern California (1981 to June 2011). *Bulletin of the Seismological Society of America* 102(5): 2239-2244.

Helmstetter, A., Kagan, Y. Y. & Jackson, D. D. (2007). High-resolution Time-independent Grid-based Forecast for M≥5 Earthquakes in California. *Seis. Res. Lett.* **78** (1), 78–86.

Hsu, Y.-J., Yu, S.-B., Loveless, J. P., Bacolcol, T., Solidum, R., Luis, A. Jr., Pelicano, A. & Woessner, J. (2016). Interseismic deformation and moment deficit along the Manila subduction zone and the Philippine Fault system. *J. Geophys. Res.* **121**(10), 7639-7665.

Hutton, K., Woessner, J. & Hauksson, E. (2010). Earthquake monitoring in southern California for seventy-seven years (1932–2008). *Bull. Seis. Soc. Am.* **100**(2), 423-446.

Jackson, D.D. & Kagan, Y. Y. (1999). Testable Earthquake Forecasts for 1999. *Seis. Res. Lett.* **70**(4), 393-403.

Leon, L. A., Christofferson, S. A., Dolan, J. F., Shaw. J. H. & Pratt, T. L. (2007). Earthquake-by- earthquake fold growth above the Puente Hills blind thrust fault, Los Angeles, California: Implications for fold kinematics and seismic hazard. *J. Geophys. Res.* **112**(B3).

Leon, L. A., Dolan, J. F., Shaw, J. H. & Pratt, T. L. (2009). Evidence for large Holocene earthquakes on the Compton thrust fault, Los Angeles, California. *J. Geophys. Res.* **114**(B12).

Lin, J. & Stein, R. S. (1989). Coseismic Folding, Earthquake Recurrence, and the 1987 Source Mechanism at Whittier Narrows, Los Angeles Basin, California. *J. Geophys. Res.* **94**(B7): 9164-9632.

Marsan, D. & Lengline, O. (2008). Extending Earthquakes' Reach Through Cascading. *Science* **319**, 1076-1079.

Marshall, S. T., Cooke, M. L. & Owen, S. E. (2009). Interseismic deformation associated with three-dimensional faults in the greater Los Angeles region, California. *J. Geophys. Res.* **114**(B12).

Marshall, S. T., Funning, G. J. & Owen, S. E. (2013). Fault slip rates and interseismic deformation in the western Transverse Ranges, California. *J. Geophys. Res.* **118**(8), 4511-4534.

Matthews, M. V., Ellsworth, W. L. & Reasenberg, P. A. (2002). A Brownian model for recurrent earthquakes, *Bull. Seis. Soc. Am.* **92**(6), 2233-2250.

Mavrommatis, A. P. & Segall, P. & Johnson, K. M. (2014). A decadal-scale deformation transient prior to the 2011 Mw9.0 Tohoku-oki earthquake. *Geophys. Res. Lett.* **41**, 4486-4494, doi:10.1002/2014GL060139.

McCalpin, J. & Nishenko, S. (1996). Holocene paleoseismicity, temporal clustering, and probabilities of future large (M> 7) earthquakes on the Wasatch fault zone, Utah. *J. Geophys. Res.* **101**(B3), 6233-6253.

Meade, B. J. & Hager, B. H. (2005). Spatial localization of moment deficits in southern California. *J. Geophys. Res.* **110**(B4).

Michel, S., Avouac, J.-P. Jolivet, R. & Wang, L. (2018). Seismic and Aseismic Moment Budget and Implication for the Seismic Potential of the Parkfield Segment of the San Andreas Fault. *Bull. Seis. Soc. Am.* **108**(1), 19-38.

Molnar, P. (1979). Earthquake recurrence intervals and plate tectonics. *Bull. Seis. Soc. Am.* **69**(1), 115-133 (1979).

Reid, H.F. (1910). The Mechanics of the Earthquake. *The California Earthquake of April 18, 1906; Report of the State Investigation Commission* (Carnegie Institution of Washington, Washington, D.C.).

Riel, B. V., Simons, M., Ponti, D., Agram, P. & Jolivet, R. (2018). Quantifying ground deformation in the Los Angeles and Santa Ana coastal basins due to groundwater withdrawal. *Water Resources Research* **54**(5), 3557-3582.

Rockwell, T., Lindvall, S., Herzberg, M., Murbach, D., Dawson, T., & Berger, G. (2000). Paleoseismology of the Johnson Valley, Kickapoo, and Homestead Valley faults: Clustering of earthquakes in the eastern California shear zone. *Bull. Seis. Soc. Am.* **90**(5), 1200-1236.

Rollins, C., Avouac, J-P., Landry, W., Argus, D. F. & Barbot, S. D. (2018). Interseismic strain accumulation on faults beneath Los Angeles, California. *J. Geophys. Res.* **123**(8), 7126-7150.

Rong, Y., Jackson, D. D., Magistrale, H. & Goldfinger, C. (2014). Magnitude Limits of Subduction Zone Earthquakes. *Bull. Seis. Soc. Am.* **104**(5): 2359-2377.

Rubin, C. M., Lindvall, S. C. & Rockwell, T. K. (1998). Evidence for large earthquakes in metropolitan Los Angeles. *Science* **281**(5375), 398-402.

SCEDC, Southern California Earthquake Data Center (*California Institute of Technology, Pasadena, CA)*. Dataset, doi:10.7909/C3WD3xH1 (2013).

Shaw, J. H. & Suppe, J. (1996). Earthquake hazards of active blind-thrust faults under the central Los Angeles basin, California. *J. Geophys. Res.* **101**(B4), 8623-8642.

Shen, Z. K., Jackson, D. D. & Kagan, Y. Y. (2007). Implications of Geodetic Strain Rate for Future Earthquakes, with a Five-Year Forecast of M5 Earthquakes in Southern California. *Seis. Res. Lett.* **78**(1).

Stein, R. S. & Yeats, R. S. (1989). Hidden Earthquakes. *Scientific American* **260**(6), 48-57.

Stevens, V. & Avouac, J. P. (2016). Millenary Mw> 9.0 earthquakes required by geodetic strain in the Himalaya. *Geophys. Res. Lett.* **43**(3), 1118-1123.

Stevens, V. & Avouac, J. P. (2017). Determination of Mmax from Background Seismicity and Moment Conservation. *Bull. Seis. Soc. Am*. **107**(6), 2578-2596.

Toppozada, T. R. & Branum, D. M. (2002). California M≥5.5 earthquakes, history and areas damaged. *International Handbook of Earthquake and Engineering Seismology* (Academic Press, Cambridge, MA).

Tsang, L. L. H. & Meltzner, A. J. & Hill, E. M. & Freymueller, J. T. & Sieh, K. (2015). A paleogeodetic record of variable interseismic rates and megathrust coupling at Simeulue Island, Sumatra. *Geophys. Res. Lett.* **42**, 10,585-10,594, doi:10.1002/2015GL066366.

Wells, D. L. & Coppersmith, K. J. (1994). New empirical relationships among magnitude, rupture length, rupture width, rupture area, and surface displacement. *Bull. Seis. Soc. Am.* **84**(4), 974-1002.

Yerkes, R. F. (1985). Geologic and Seismologic Setting. *Evaluating Earthquake Hazards in the Los Angeles Region – An Earth-Science Perspective.* U.S. Geol. Survey Professional Paper 1360, 25-42.

Zoback, M., Zoback, M. L., Mount, V., Suppe, J., Eaton, J. P., Healy, J. H., Oppenheimer, D., Reasenberg, P., Jones, L., Raleigh, B., Wong, I. G., Scotti, O., & Wentworth, C. (1987). New evidence on the state of stress of the San Andreas fault system. *Science* **238**(4830), 1105-1111.

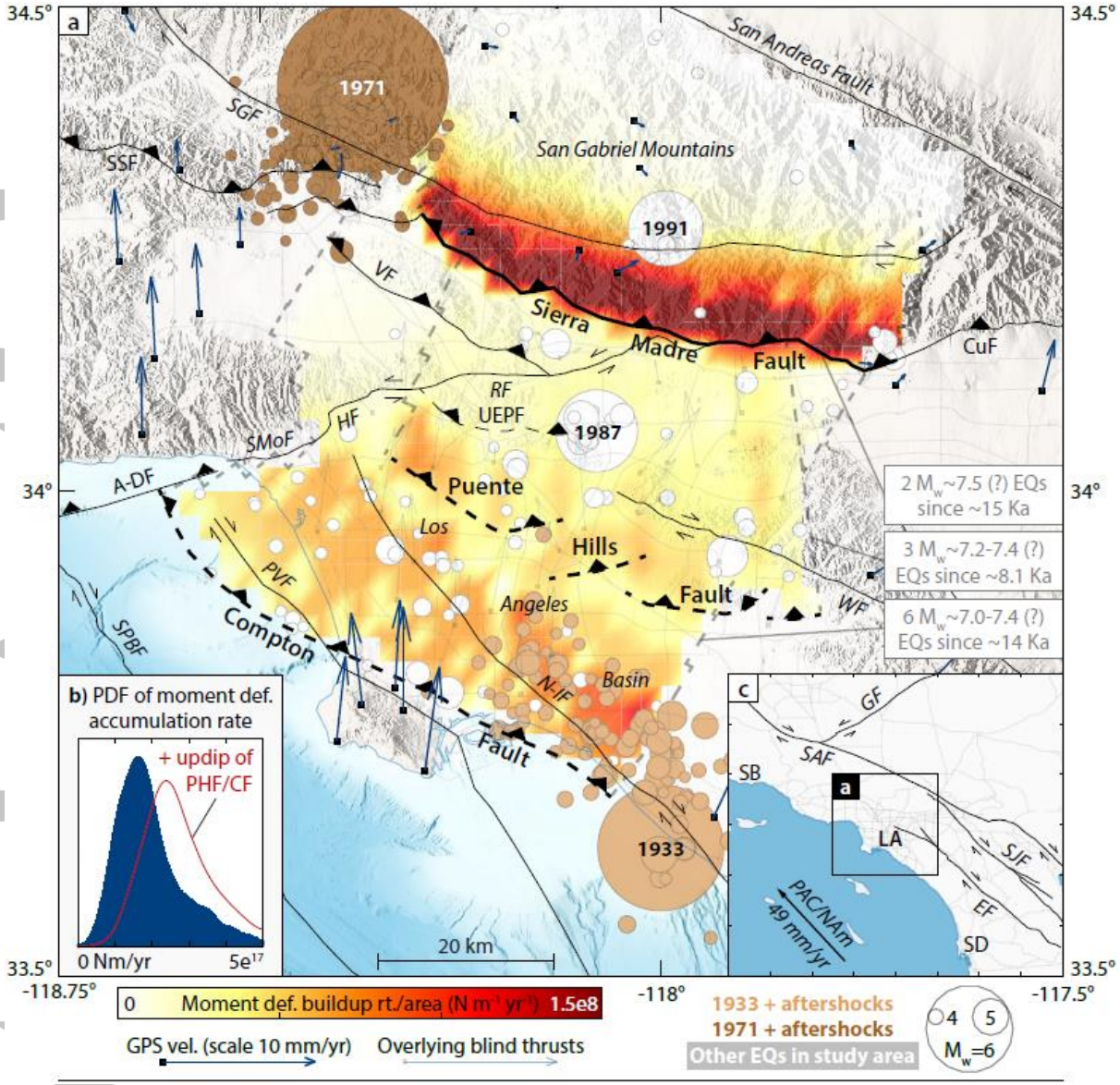

Figure 1. a) N-S shortening, seismic moment deficit buildup, and earthquakes in central LA. Blue arrows (translucent in study area) are GPS velocities relative to the San Gabriel Mountains corrected for anthropogenic deformation and interseismic locking on the San Andreas system [Argus et al., 2005]. Paleoearthquakes on the Sierra Madre, Puente Hills and Compton faults are respectively from Rubin et al. [1998] and Leon et al. [2007, 2009]. Color shading is geodetically inferred distribution of moment deficit buildup rate associated with these three faults [Rollins et al., 2018]. Study area is defined by the three faults and an inferred master decollement (thin dashed lines). 1932-2017 earthquake locations and magnitudes are from the SCEDC catalog. The 1933 Long Beach and 1971 Sylmar earthquakes and their aftershocks (brown circles) occurred on the periphery of the study area. Black lines are upper edges of faults, dashed for blind faults. Faults: SGF: San Gabriel; SSF: Santa Susana; VF: Verdugo; CuF: Cucamonga; A-DF: Anacapa-Dume; SMoF: Santa Monica; HF: Hollywood; RF: Raymond; UEPF: Upper Elysian Park; ChF: Chino; WF: Whittier; N-IF: Newport-Inglewood; PVF: Palos Verdes; SPBF: San Pedro Basin. **b)** PDF of moment deficit buildup rate from Rollins et al. [2018]. Folding updip of the Puente Hills and Compton faults is assumed anelastic; if it were elastic, the PDF would be the red curve. **c)** Tectonic setting. Arrow pairs show slip senses of major faults. Offshore arrow is Pacific Plate velocity relative to North American plate [Kreemer et al., 2014]. SB: Santa Barbara. LA: Los Angeles. SD: San Diego. Faults: GF: Garlock; SJF: San Jacinto; EF: Elsinore.

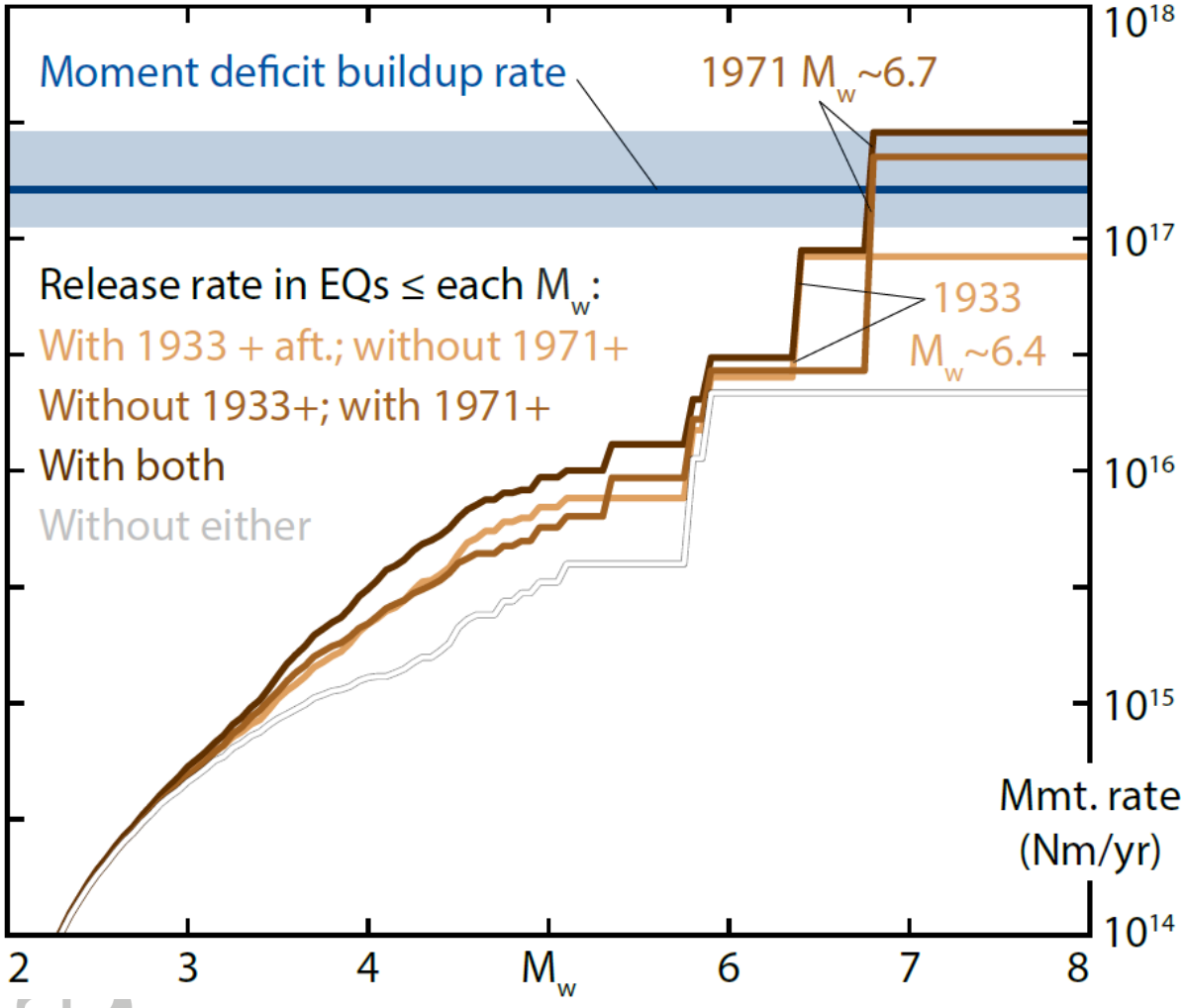

Figure 2. Comparison, over the 86-year timespan of the SCEDC catalog, of moment deficit buildup rate (mode and 16th-84th percentiles of PDF) with moment release rate in earthquakes in Figure 1. Brown and white lines denote, at each magnitude, the cumulative moment release per year by earthquakes that do not exceed that magnitude. We consider four versions of the instrumental catalog as indicated.

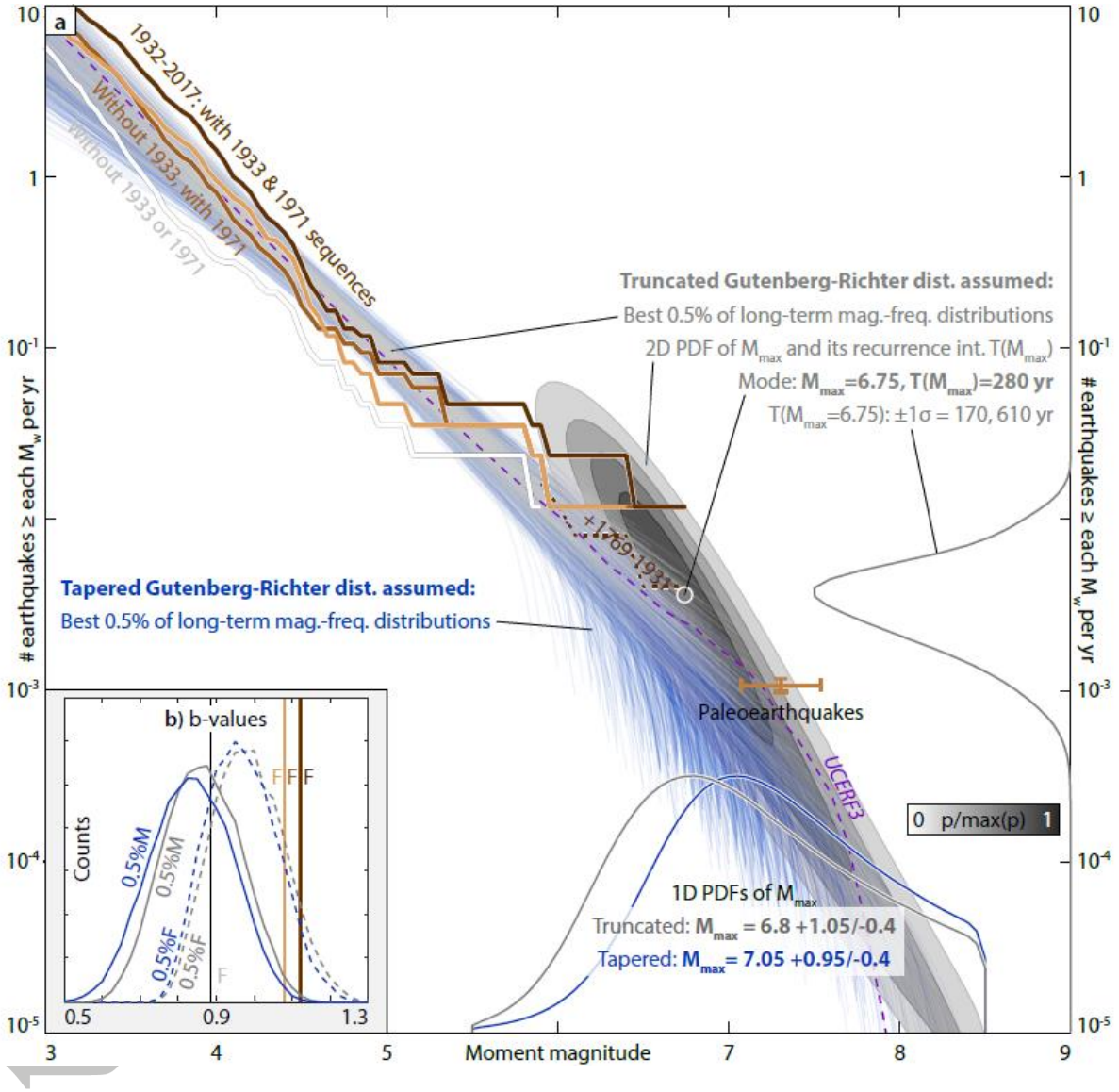

Figure 3. a) Preferred estimates of long-term-average earthquake likelihoods (in Gutenberg-Richter space), assuming that mainshocks obey a truncated (gray) or tapered (blue) G-R MFD and are accompanied by aftershocks obeying a truncated G-R MFD and "Bath's law" plus postseismic deformation. Brown lines are cumulative MFDs of the four versions of the instrumental catalog. Thin translucent lines are full MFDs (including aftershocks) of the best-fitting 0.5% of models in the truncated (gray) and tapered (blue) cases. Gray shape is the 2D PDF of the maximum earthquake's magnitude and recurrence interval assuming a truncated G-R distribution. Brown errorbars show aggregate recurrence interval and magnitudes of paleoearthquakes in Figure 1. Dashed purple line is cumulative UCERF3 nucleation MFD from all faults in study area (Supporting Information S7). **b)** Histograms of b-values in the best-fitting 0.5% of truncated (gray) and tapered (blue) models. Solid lines are intrinsic model parameter *b* that governs mainshocks (M) and individual aftershock sequences; dashed lines are maximum-likelihood [Aki, 1965] b-values of the full (F) long-term MFDs of the same models (including aftershocks) at M_c=3.5; brown lines are maximum-likelihood b-values of four versions of the instrumental catalog at M_c=3.5.

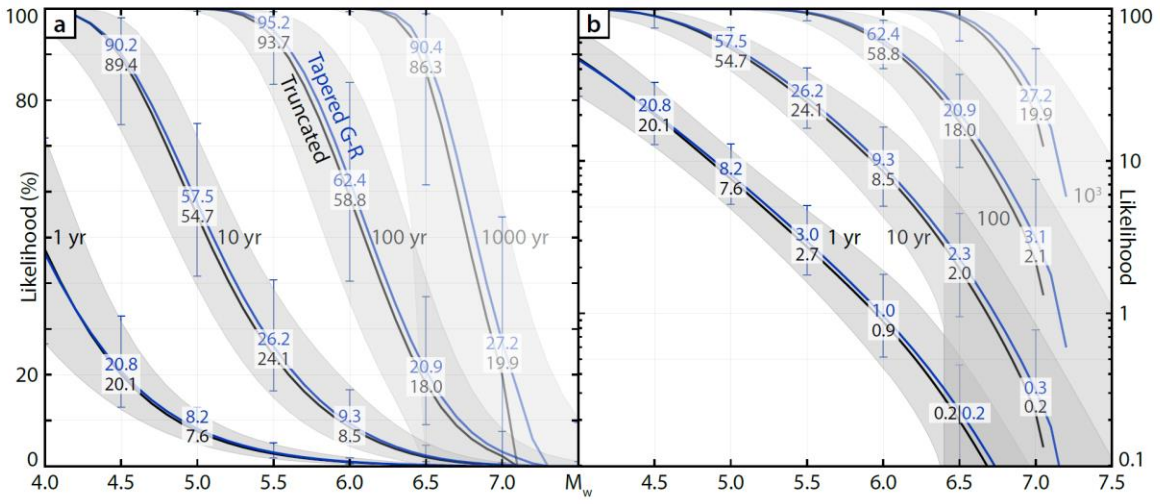

Figure 4. Likelihoods (plotted with a linear **(a)** or logarithmic **(b)** y-axis) of observing at least one mainshock of or exceeding a given magnitude in the study area over a 1-, 10-, 100- or 1000-year period as indicated, assuming that individual mainshocks obey a Poisson process. Gray lines and shading are weighted median and weighted 16th-84th-percentile likelihoods assuming a truncated G-R distribution. Blue lines and errorbars are the same assuming a tapered G-R distribution.